Open access • Journal Article • DOI:10.1063/1.1710860

Application of density functional theory to capillary phenomena in cylindrical mesopores with radial and longitudinal density distributions — Source link

E. A. Ustinov, Duong D. Do

Institutions: Saint Petersburg State Polytechnic University

Published on: 06 May 2004 - Journal of Chemical Physics (American Institute of Physics)

Topics: Phase transition

Application of density functional theory to capillary phenomena in cylindrical mesopores with radial and longitudinal density distributions

E. A. Ustinov and D. D. Do

Citation: The Journal of Chemical Physics **120**, 9769 (2004); doi: 10.1063/1.1710860
View online: http://dx.doi.org/10.1063/1.1710860
View Table of Contents: http://scitation.aip.org/content/aip/journal/jcp/120/20?ver=pdfcov
Published by the AIP Publishing

Application of density functional theory to capillary phenomena in cylindrical mesopores with radial and longitudinal density distributions

E. A. Ustinov
Saint Petersburg State Technological Institute (Technical University), 26 Moskovky Prospect, St Petersburg, Russia

D. D. Do
Department of Chemical Engineering, University of Queensland, St. Lucia, Queensland 4072, Australia

(Received 11 August 2003; accepted 25 February 2004)

In this paper, we applied a version of the nonlocal density functional theory (NLDFT) accounting radial and longitudinal density distributions to study the adsorption and desorption of argon in finite as well as infinite cylindrical nanopores at 87.3 K. Features that have not been observed before with one-dimensional NLDFT are observed in the analysis of an inhomogeneous fluid along the axis of a finite cylindrical pore using the two-dimensional version of the NLDFT. The phase transition in pore is not strictly vapor–liquid transition as assumed and observed in the conventional version, but rather it exhibits a much elaborated feature with phase transition being complicated by the formation of solid phase. Depending on the pore size, there are more than one phase transition in the adsorption–desorption isotherm. The solid formation in finite pore has been found to be initiated by the presence of the meniscus. Details of the analysis of the extended version of NLDFT will be discussed in the paper. © *2004 American Institute of Physics.* [DOI: 10.1063/1.1710860]

I. INTRODUCTION

For the last decade there is a significant progress in understanding of capillary phenomena, probably, due to the following two factors: the discovery of highly ordered adsorbents MCM-41 silicas with a well-defined cylindrical pore structure[1–3] and the wider applications of sophisticated molecular models, one of which is the nonlocal density functional theory (NLDFT).[4–13] It was shown that classical models, even those based on rigorous thermodynamic approach like the Broekhoff and De Boer method,[14,15] are not accurate enough and is applicable only to wide cylindrical pores.[16] Simpler models using Kelvin equation[17] need special attention. The Barrett, Joyner, and Halenda method of pore size distribution analysis[18] based on this equation significantly underestimates pore diameters and may lead to correct results only for pores having diameter larger than 20 nm.[19] Some improvement of the Kelvin equation was proposed by Jaroniec *et al.*[20–22] They modified it for the case of semispherical meniscus and showed that the new equation named KJS (Kruk, Jaroniec, and Sayari) is applicable to the adsorption branch of nitrogen and argon isotherms on MCM-41. Note that the Kelvin equation derived for the semispherical meniscus yields pressure at which capillary evaporation occurs. This is known to associate with thermodynamic equilibrium,[14,23,24] and the pressure at which capillary evaporation occurs is known as the equilibrium vapor–liquid transition pressure. Because hysteresis is usually present, this suggests that capillary condensation does not occur at vapor–liquid equilibrium transition pressure, but rather at a vaporlike spinodal point, where adsorbed phase loses its mechanical stability. On the contrary, the capillary evaporation may occur at a pressure, which is less than the equilibrium transition pressure. This shift of the evaporation pressure is ascribed to single-pore blocking effect.[25] The mechanism of capillary evaporation from an open-ended cylindrical pore is still not completely understood. It was found that the steepness of desorption isotherms increases with a decrease in pore diameter, and such steepness is not due to the narrow pore size distribution.[20] It is also well known that there is the lower limit of pressure above which hysteresis is observed.[26] For nitrogen at 77 K this lower limit of relative pressure is about 0.4, while for argon it is 0.34 at 87.3 K.[27] So far there are no rigorous models that could describe all features of adsorption and desorption isotherms and not resort to any hypothetical assumptions even in the simplest case of cylindrical pores of MCM-41. For example, the Broekhoff and de Boer theory could not describe the reversibility of adsorption and desorption isotherms.[19] Nonlocal density functional theory does predict reversibility, but gives markedly lower value for the critical pore diameter of hysteresis loop than that observed experimentally. For example, in the case of nitrogen adsorption at 77 K the NLDFT predicts a critical pore diameter of 2 nm[19] instead of 4 nm, which is observed experimentally. This difference is still not completely understood. Even for larger pores there are some deviations between estimation of pore diameters determined with NLDFT and with x-ray diffraction data,[16] which requires further discussion. One of the reasons hampering to quantitatively describe experimental isotherms might be associated with the use of the one-dimensional version of the NLDFT both for slit and cylindrical pores that implies the adsorbed phase to be homogeneous along the pore walls surface. However, pore filling and evaporation occur through the formation of meniscus, which could be described only in the framework of two-dimensional (2D) or three-dimensional (3D) configuration of the pore. Hereafter we apply the terms one-

dimensional and two-dimensional versions of the NLDFT or solutions just for simplicity, meaning that in all cases the real adsorption process occurs in three-dimensional space. So the term 1D version of the NLDFT in the case of cylindrical pore denotes that there is only one independent variable, namely radius, along which the change of adsorbed phase density can be observed, while in longitudinal direction the adsorbed phase is homogeneous. Also, it should be kept in mind that the process of solidification of the adsorbed fluid (which could occur in pores) cannot be described by the 1D model. It is interesting to note that isotherms obtained for model cylindrical pores by the one-dimensional NLDFT and in Monte Carlo simulations were shown to agree quite well[16] although MC simulation is a three-dimensional task. The reason of such an agreement could be associated with the size of the simulation cell, which is not large enough (typically 10 collision diameters[28,29]) to allow three-dimensional molecular rearrangement. On the other hand, the use of relatively large simulation cell of 30×30 collision diameters in slit pores does lead to the solidification.[30] It should be noted that an important factor is the roughness of pore walls. Thus, in GCMC simulations of xenon adsorption in a silicalike adsorbent[31] a very long simulation cell (up to 108 nm along the cylindrical pore axis) was used. In this work the authors generated an amorphous pore wall surface by a Lennard-Jones frozen liquid for oxygen atoms, which allowed them to model a rough surface. In this case no solidification was observed. The aim of this paper is to extend the NLDFT to the two-dimensional case of a cylindrical pore in order to obtain a better insight of the mechanism of adsorption and desorption. We consider adsorption isotherms for finite and infinite pores for the case of argon adsorption in cylindrical carbon nanotubes at 87.3 K.

II. THE STATE OF INVESTIGATIONS OF CAPILLARY PHENOMENA FROM THE VIEWPOINT OF DENSITY FUNCTIONAL THEORY

The background of the nonlocal density functional theory and its application to the analysis of adsorption in pores of different shape are well described in the literature.[4–13] The basic idea of this theory is to find the density distribution in molecular scale inside a system (for example, confined fluids in pore, and the vapor–liquid interface) such that a general thermodynamic condition of equilibrium is satisfied. For open isothermal systems of constant volume, which conform to a grand canonical ensemble, the equilibrium condition corresponds to the minimum of the grand thermodynamic potential Ω. Most applications of the NLDFT to adsorption rely on minimization of this thermodynamic function because real pore systems can exchange mass and energy with the surrounding. In this case the density distribution is obtained at a specified chemical potential (which is equivalent to specifying the bulk phase pressure) and temperature. By such a way one can generate a set of isotherms corresponding to pores of different size. For sufficiently large pores the calculated isotherms exhibit a sharp increase in the adsorption amount at the point known as the equilibrium phase transition pressure. At this point the grand potentials of the liquidlike and the vaporlike coexisting phases are equal. For pressures greater than the equilibrium transition pressure the local minimum of the grand potential corresponding to the liquidlike phase is lower than that of the vaporlike phase. It has been observed in many experimental systems that the sharp jump in adsorption amount of the adsorption branch of the isotherm occurs at a pressure greater than the equilibrium transition pressure. The classical NLDFT cannot describe this pressure, and to resolve this problem the NLDFT was recently adapted[16,32] to a canonical ensemble, in the framework of which a pore is considered as a close system. In this case the thermodynamic equilibrium corresponds to the minimum of the Helmholtz free energy. This has the advantage that the adsorbate confined in a pore is stable. The isotherm for sufficiently large pores has an S-shape and the backward branch of the isotherm is bounded by the vaporlike and liquidlike spinodal points. At these points the system loses its stability and, consequently, they can be considered as the limits of metastable branches of the isotherm. The metastable adsorption branch connects the vaporlike equilibrium transition point and the vaporlike spinodal point. Analogously, the metastable desorption branch lies to the left of the equilibrium transition point between the liquidlike equilibrium transition point and the liquidlike spinodal point. It has been argued in the literature that during adsorption the bulk pressure could approach the vaporlike spinodal point, whereas the desorption branch terminates at the equilibrium transition point, resulting in a hysteresis loop. Neimark and co-workers[29,33] pointed out that in the case of sufficiently large pores the capillary condensation occurs at the vaporlike spinodal point. They denoted this the developed hysteresis loop, to distinguish from the developing loop when the capillary condensation occurs before the vaporlike-spinodal point. The latter occurs in smaller pores. The authors treated isotherms of nitrogen and argon on different ordered mesoporous silica and came to the conclusion that the NLDFT properly and quantitatively describes adsorption and desorption isotherms.[19,33,34] In this case the capillary condensation occurs before the bulk pressure reaches the spinodal point. The reason is that the potential barrier separating the metastable state from the true equilibrium state may be overcome due to fluctuations in the adsorbed density.[29] This argument suggests that the potential barrier grows with pore diameter. To estimate the probability of spontaneous jump from the metastable adsorption branch of the isotherm to the stable desorption branch, Vishnyakov *et al.*[29] suggested a qualitative criterion in the form of Arrhenius equation. Further efforts are needed to clarify the mechanism of phase transition in pores. Our viewpoint is that such a transition occurs through a formation of a fluid structure that is not one dimensional as commonly assumed in all previous NLDFT work. In this paper we consider the two-dimensional fluid structure in confined space by applying the two-dimensional version of the NLDFT.

III. MODEL

A. Nonlocal density functional theory in 2D space

In this paper we use the Tarazona's version of NLDFT.[4–6] Attractive part of intermolecular interaction is

modeled by the Weeks–Chandler–Andersen equation[35] with the usual assumption of the mean field approximation. The repulsive part of the Helmholtz free energy is described by the Carnahan–Starling equation for the equivalent hard sphere fluid.[36] Thus, the intrinsic Helmholtz free energy comprises of the ideal, attractive and repulsive parts. All mathematical details have been described in the literature and can be found elsewhere (see Ref. 37 for a thorough review). The weighted functions for the Tarazona's smoothed density approximation were given in vector form.[4] In the case of cylindrical geometry these weighted functions are function of three parameters, which are the distance from the cylinder axis to the center of a given molecule, and projections of the distance between the given molecule and any other molecule on radial and longitudinal directions. This three-parametric discrete set of the weighted functions is calculated and tabulated for further use in the subsequent adsorption calculations. In this paper we explore the canonical version of the 2D NLDFT, that is we will search for the density distribution corresponding to the minimum of the Helmholtz free energy of the system. Since the Helmholtz free energy is in the form of quadrature, its numerical evaluation can be done by dividing the radial coordinate and axial coordinate into equal segments whose thickness is one-tenth of the collision diameter. Each ring has a mass that is proportional to the fluid density at given radius and z coordinate along the axis.

In canonical ensemble the total number of particle in a pore is specified. With this constraint the minimization of the Helmholtz free energy leads to the condition that all partial derivatives of the Helmholtz free energy with respect to local density are equal to the same value, which is the chemical potential. The simplest way of calculations is to choose one point in the system, where the local density is determined by the set of the remaining values of the density while maintaining the total amount in the system constant. The partial derivative of the Helmholtz free energy with respect to this density is the chemical potential. But this way requires some precautions to avoid negative density at the specified point and numerical instability of calculations. One logical way is to define the chemical potential of a closed system as follows:

$$\mu = -\omega kT \ln(\xi/a), \tag{1}$$

where

$$\xi = \int \rho \exp\left[-\frac{1}{\omega kT}\frac{\partial F}{\partial \rho}\right] dr,$$
$$a = \int \rho \, dr. \tag{2}$$

In these equations F is the Helmholtz free energy, which is a function of coordinates and the set of local and Tarazona's smoothed densities; ρ is the local density; a is amount adsorbed in the pore, which is specified in canonical ensemble; ω is an arbitrary number greater than unity, which is introduced to stabilize the iterative procedure. In our calculations ω was between 20 and 40. At each iteration the chemical potential is recalculated by Eq. (1) and then the next iterated local density is determined by

$$\rho^{(n+1)} = \left[\rho \exp\left(\frac{\mu - \partial F/\partial \rho}{\omega kT}\right)\right]^{(n)}, \tag{3}$$

where n is the number of iteration. At equilibrium conditions all partial derivatives $\partial F/\partial \rho$ equal to the chemical potential. In this case local densities will not further change.

To analyze the nonuniform system along the axis of a cylindrical pore we consider a cell, which is a part of the cylindrical pore, and the cell length is of the order of 10 times the collision diameters. In the case of uniform density distribution the solution completely coincides with that corresponding to the one-dimensional DFT, which confirms the correctness of our approach. To model formation of a nonuniform structure along the radius and the axis we use sinusoidal initial conditions. It stimulated formation of a bridge or gap that could be stable or unstable depending on the average loading and other factors, which will be discussed below.

B. Solid–fluid potential for infinite and finite cylindrical pore

We model the pore walls of cylindrical pores as a set of coaxial cylindrical graphite layers with the same interlayer spacing Δ (0.335 nm) and surface density ρ^s (38.19 nm^{-2}) as in the case of the graphitized carbon black. The contribution of each layer to the solid–fluid potential energy was calculated as integral of Lennard-Jones (LJ) potential energy between an adsorbed molecule and all carbon atoms on the cylindrical surface of this layer. The solution of this task for the cylinder of infinite extent has been obtained in the form of hypergeometric function.[38] However, we used a direct approach of integrating the LJ pairwise potential over the surface of the carbon wall. This approach is more general than the analytical approach because it can be applied readily to the case of finite pores. For example, in the case of a single cylindrical layer of infinite extent in the longitudinal direction this potential may be written as follows:

$$u(r,R) = 4\rho^s \epsilon_{sf} \int \left(\frac{\sigma_{sf}^{12}}{|\mathbf{r}-\mathbf{r}'|^{12}} - \frac{\sigma_{sf}^{6}}{|\mathbf{r}-\mathbf{r}'|^{6}}\right) d\mathbf{r}'$$
$$= 3\pi\rho^s \epsilon_{sf}\sigma_{sf} R \int_0^{\pi} \left(\frac{21}{32}\frac{\sigma_{sf}^{11}}{x^{11}} - \frac{\sigma_{sf}^{5}}{x^{5}}\right) d\alpha \tag{4}$$

with

$$x = (R^2 + r^2 - 2rR\cos\alpha)^{1/2}.$$

Here R is the radius of the cylindrical layer and r is the radial distance of a given point inside the cylinder from its axis. As is seen from Eq. (4), integrating over the cylindrical layer surface is reduced to an integral of one dimension. Such a transformation can be applied for the case of finite pore (see the Appendix for further details). The direct numerical approach is very fast and the results of integration can be tabulated for subsequent adsorption calculations.

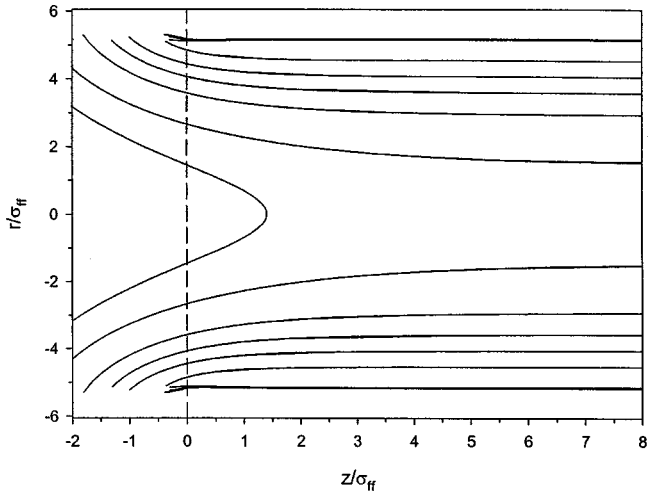

FIG. 1. Lines of constant solid–fluid potential in a finite carbon nanotube of 3 nm diameter. Dashed line is the entrance to the pore. Solid lines are plotted for the following values of u/kT: -0.1, -0.2, -0.5, -1, -2, -5.

The finite pore in this paper is chosen as an active part of an infinite pore where solid–fluid potential is nonzero and it is zero otherwise. We considered the application of 2D NLDFT to the finite and infinitely long cylindrical pore. Figure 1 shows equipotential lines in the proximity of the edge of the semi-infinite cylinder of 4 nm diameter. The dashed line denotes the boundary between the active and inactive parts of the pore. It is seen from the figure that the potential field substantially differs in the region of the mouth of the pore and deviates from uniform distribution along the pore axis. The potential becomes weaker in this region, however, it does not equal zero outside the pore. Inside the pore the potential becomes nearly uniform at a distance of about 3–4 collision diameters from the pore edge. We use this potential to model adsorption in finite pores.

IV. RESULTS

A. Adsorption of argon in finite cylindrical pores

Adsorption in finite cylindrical pores is more complicated compared to one-dimensional solution for a cylindrical pore of infinite extent. However, it is essential to consider the two-dimensional finite pore as it models real pore better than the one-dimensional infinite pore does. The latter is merely an asymptotic case of finite pore, and as such it could not exhibit behaviors that finite pores do.

Molecular parameters for argon are taken from the paper of Ravikovitch and Neimark.[39] For the collision diameter and the hard sphere diameter the authors gave values 0.3305 nm and 0.338 nm, respectively. The value of the potential well depth ϵ_{ff}/k was taken as 118.05 K. For the solid–fluid potential ϵ_{sf}/k we used the value 57.95 K, which corresponds to the best fit of the argon isotherm on graphitized carbon black at 87.3 K. Chemical potential was calculated by Eq. (1) and at equilibrium it is equal to the partial derivative of the Helmholtz free energy with respect to density. Given the chemical potential, the equilibrium bulk phase pressure was calculated by the equation of state, which is a combination of the Carnahan–Starling equation and the Weeks–Chandler–Andersen scheme for attractive forces in the case of homogeneous fluid. The results for argon adsorption at 87.3 K in the cylindrical pores of 3 and 4 nm diameters are shown in Fig. 2 in the form of the pore average density versus reduced pressure. The density in this paper is defined as $\rho = N/(L\pi R^2)$, where N is the number of adsorbed moles, L and R are the length and radius of the pore, respectively. Dashed line $ABCDEFG$ is obtained from the 1D canonical version of NLDFT. The features of this curve are typical for the 1D case of canonical ensemble and discussed elsewhere.[16] Part BC is the metastable adsorption branch. The backward branch CDE between vaporlike and liquidlike spinodal points is unstable in open systems. The part EF is the metastable desorption branch. Vertical solid line BDF corresponds to the equilibrium phase transition, where the equality of the grand thermodynamic potentials between the lower and the upper points (B and F) of this line holds. The curve $ABDFG$ has been obtained by 1D grand canonical NLDFT. Parts AB and FG calculated by the canonical and grand canonical NLDFT completely coincide, which confirms the credibility of the results. The results calculated by

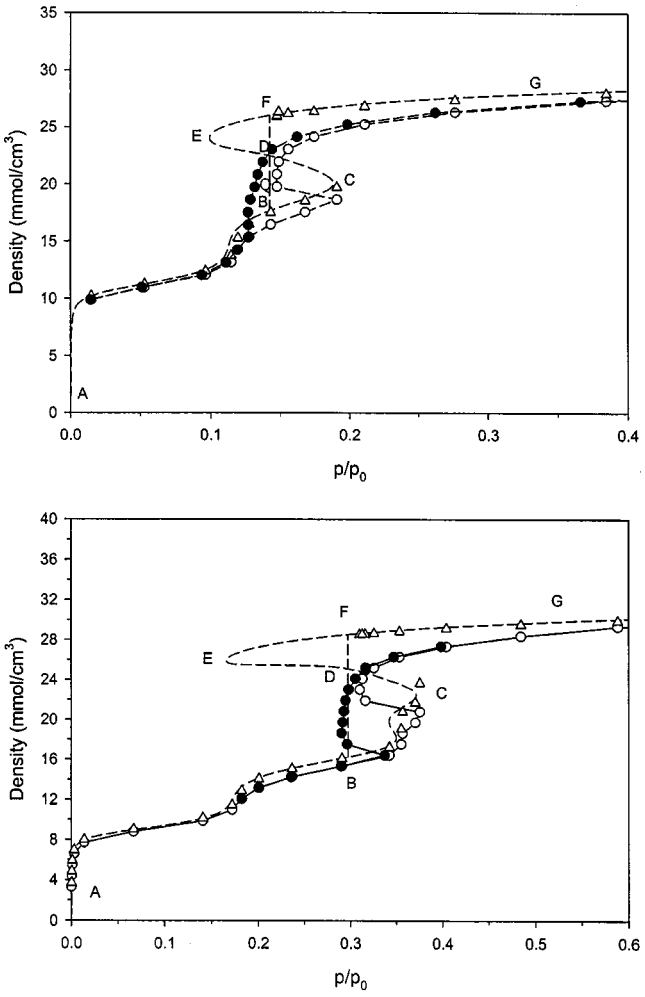

FIG. 2. Argon isotherm in cylindrical pore of 3 nm (a) and 4 nm (b) diameter at 87.3 K. Curves $ABDFG$ are calculated by 1D grand canonical NLDFT. Curves $ABCDEFG$ are calculated by 1D canonical NLDFT. Triangles correspond to the center of finite pore during adsorption. Circles (white for adsorption and black for desorption) are plotted for the average density of the adsorbed phase.

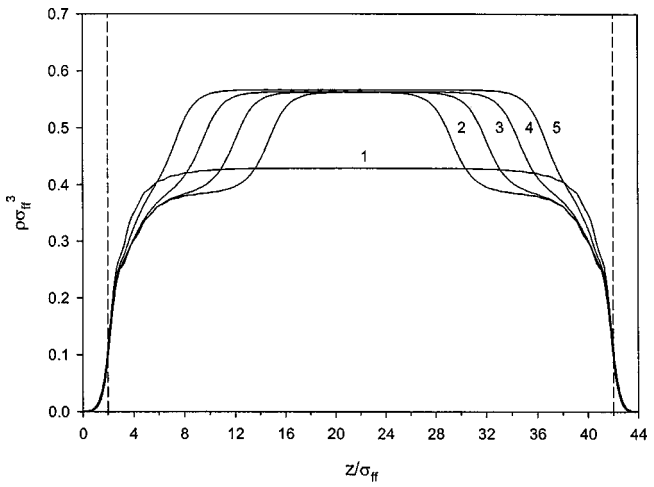

FIG. 3. Density distribution of argon along the finite cylindrical pore of 3 nm diameter. Bulk pressure p/p_0: (1) 0.1909, (2) 0.1453, (3) 0.1452, (4) 0.1455, (5) 0.1541. Average density (mmol/cm^3): (1) 18.624, (2) 19.721, (3) 20.817, (4) 21.898, (5) 23.002. The adsorbed phase is split if the average argon density exceeds 19 mmol/cm^3.

the 2D version of the density functional theory for the finite pore of the same diameter and length of 40 collision diameters are presented as symbols (○ and △). Circle symbols denote the density averaged over the total pore volume, while triangles correspond to the average density in the section of the pore away from the boundary. In the central part of the pore away from its edges the density distribution in the axial direction is nearly uniform, and it agrees with that obtained for the infinitely long pore by 1D NLDFT. Results presented as circles are lower than those described by triangle symbols. This is because the loading is lower in the proximity of the pore edges, where the solid–fluid interaction is weaker. The most interesting feature is that after the vaporlike spinodal point has been reached the pressure decreases rapidly towards the equilibrium transition pressure and never goes to the left of this point. At this instant the average density in the central section of the pore is approximately the loading on the desorption branch at the liquidlike equilibrium transition point (triangle symbol next to the point F). This suggests a formation of a meniscus separating the liquid section of the pore (the central section) and the vaporlike phase (near the pore mouth). The vaporlike section behaves like point B of the 1D solution while the liquidlike section behaves like point F on the same isotherm. The fraction of the pore occupied by the liquid phase (the central section of the pore) is estimated from the equilibrium vapor–liquid tie line BF and the position at which the phase splitting occurs [point Q in Fig. 2(b)]. The ratio of the liquid phase to vapor phase at the instant of phase splitting is BQ/FQ. As density increases, the pore fraction occupied by the vaporlike phase decreases but the pressure remains the same as the equilibrium vapor–liquid transition pressure. This continues until the fraction of the vaporlike phase approaches zero, beyond which the adsorbed phase density slowly increases due to the compression of liquid. This is clearly seen in Fig. 3 where we show the density distribution along the axis direction for the finite pore of 3 nm diameter and 40 collision diameters length (13.22 nm). Note that the density is averaged over the cross section of the pore. The curve 1 reflects uniform distribution along the pore and approximately corresponds to the vaporlike spinodal point. Small increase of the loading leads to a spontaneous split of the adsorbed phase, and at this instant the bulk phase pressure decreases and approaches the equilibrium transition pressure, suggesting the equilibrium between the two coexisting phases. In the central part of the pore dense liquidlike phase has appeared, while in regions closer to the pore edges the density has decreased slightly due to the transfer of molecules into the liquid phase in the central part. Further increase of loading leads to the increase of the liquidlike phase at the expense of pore section occupied by the vaporlike phase. Eventually, the vaporlike phase disappears and then the pressure starts to increase due to the increase of the adsorbed phase density. Thus, one can conclude that in canonical ensemble the adsorbed phase in cylindrical pore cannot be uniform in the axial direction in the region of instability between the two spinodal points. The importance of long enough simulation cell needs to be emphasized because if the cell length is short uniform density distribution would be resulted even with Monte Carlo simulation or 2D NLDFT. In this case the appearance of the liquid–vapor interface would increase the total Helmholtz free energy, which is not thermodynamically favorable.[16]

The desorption branch of the isotherm is plotted in Fig. 2, shown as filled circle symbols. We note that the desorption does not follow the metastable desorption branch. Upper parts of the adsorption and desorption branches nearly coincide. As the amount adsorbed decreases the section of the pore occupied by liquidlike phase shrinks until the two-phase coexistence becomes unstable. At this moment molecules rearrange, the liquidlike phase disappears and the pressure slightly increases for the case of 4 nm pore. However, the pressure does not reach the vaporlike spinodal point. One could expect that in the case of infinitely long pore desorption will go along the curve $GFDBA$. It is interesting to note that in the case of 3 nm diameter the desorption branch is shifted toward lower value of pressure, while in larger pore of 4 nm the evaporation pressure is very close to the equilibrium transition pressure. The reason of this feature is not quite clear and, probably, in the former case of finite pore there are two different solutions. Figure 4 shows the density distribution for the 3 nm pore at the same average density of 18 mmol/cm^3 for adsorption and desorption branches of the isotherm.

1. Freezing of argon in finite cylindrical pores

The 2D version of NLDFT developed for nonuniform density distribution along cylindrical pore axis leads to some results, which could never be obtained by the one-dimensional version. After the adsorbed phase has split into vaporlike and liquidlike phases, a molecular ordering can be observed. It is reflected in the appearance of small periodical density oscillations along the axial direction, which grow very fast with the increase of the average density. It is accompanied by the decrease in the Helmholtz free energy and increase of density of the liquidlike phase. This strong mo-

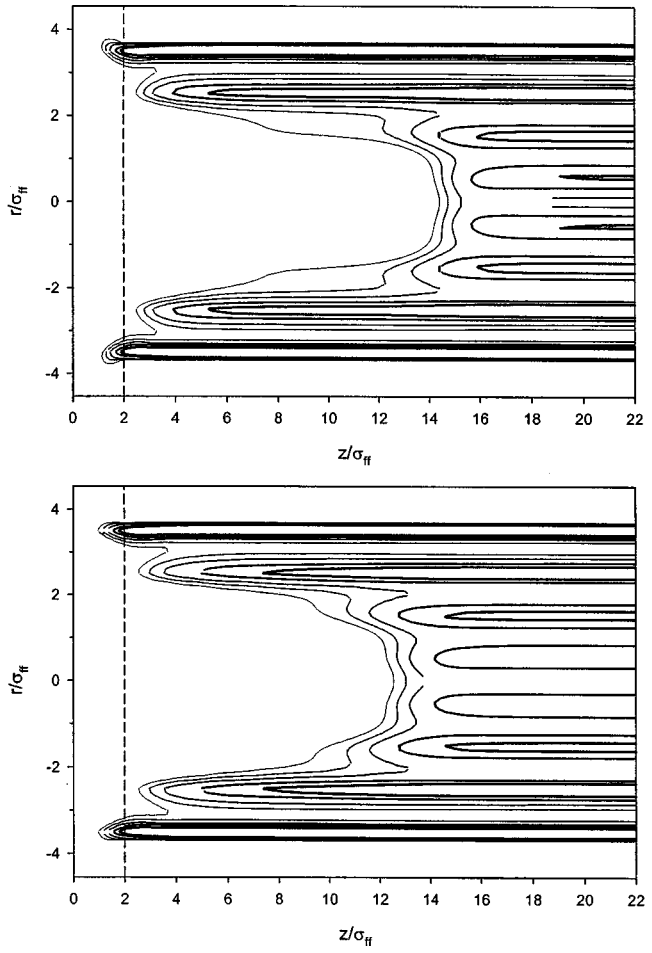

FIG. 4. The argon density distribution in the finite pore having diameter of 3 nm and length 40 collision diameters at average density of 18 mmol/cm^3. Contour lines correspond to the following values of the specified local dimensionless density $\rho\sigma_{ff}^3$: 0.05, 0.1, 0.2, 0.5, 1. (a) Adsorption; (b) desorption.

lecular ordering suggests a formation of solid argon. This interesting result does not contradict experimental and theoretical investigations of freezing in confined space. In our DFT analysis we observed the solidification at the boiling point of argon (87.29 K), which is above the triple point (83.78 K). It is commonly known that in many experimental investigations the freezing point of a fluid confined in pores is less than that in the bulk phase (for a review, see Ref. 40, part 6). However, Maddox and Gubbins[41] noted that in most experimental systems adsorbents like pore glass had weak solid–fluid potential compared to the fluid–fluid potential. Theoretical analysis of methane adsorption in carbon buckytubes[41] and experimental studies of adsorption of different species on mica surfaces[42–44] and in graphitic micropores[45] show that the freezing temperature may be significantly higher than that in the corresponding bulk phase. However, all results described below should be considered with caution. The reason is that the developed version of the NLDFT does not account for the density variations with respect to the axial angle. As a result the minimum of the Helmholtz free energy achieved in the simulation might not correspond to a global minimum, but rather a local one. Second, the application of the mean field approximation to strongly structured adsorbed phase is questionable. Even though the above simplifications do not allow us to reproduce quantitatively properties of the fluid in the bulk phase and in the adsorbed phase, it is worthy to analyze the equilibrium of the system to obtain a better insight into capillary phenomena. To judge whether the shift of freezing point is negative or positive it is necessary to calculate the bulk phase diagram and the triple point for the case of cylindrical symmetry when density is a function of the two independent variables: radius and axial distance. This will be presented in our future correspondence.

In the preceding section we presented results that were obtained by the following procedure. To suppress oscillations we smoothed density distribution in the axial direction in each 10 iterations by replacement of the density at a given point by an average of this point and its two nearest points. By such a way adsorbed argon was artificially constrained at liquidlike state against the tendency of the system to evolve into solidlike adsorbed phase. If the suppression of the density oscillation is relaxed the molecular ordering then develops resulting in an increase of the average density. This signals the phase transition from liquid to solid. This process is extremely long. During the process of calculations the chemical potential increased sharply numerous times and then gradually decreases, implicitly revealing local molecular rearrangement that leads each time to a more favorable configuration. What is significant here is that the solidification started from the regions close to the vapor–liquid boundaries. It suggests that the vapor–liquid meniscus promotes the solidification and provides necessary nucleation sites. In the case of infinite pore the process of solidification may be initiated by density fluctuations and they have to be large enough to overcome a potential barrier associated with the formation of the solid–liquid interface.

In Fig. 5 we plotted contours of constant local density corresponding to minimum of the Helmholtz free energy. The average density in this case is 27 mmol/m^3. It is seen that the hexagonal molecular structure of the adsorbed phase has been formed. The density of the solid phase is higher than that of the liquid phase, so the solidification leads to shifting of the meniscus (to retain constant loading) and the solid region toward the central part of the pore. The highest density is observed in the proximity of the pore wall, while the pore axis is void of any molecule. The latter is due to the solidification and the spacing of the pore axis is not large enough to accommodate an extra layer of molecules. We note in Fig. 5 that the meniscus is clearly defined. In the neighborhood of the interface, we also observe a transition from solidlike behavior to vaporlike behavior of the adsorbed phase.

Figure 6 shows the adsorbed phase structure in the case when the average argon density is 17 mmol/cm^3 in pore of 3 nm diameter (compared to 27 mmol/cm^3 in Fig. 5). Central part of the adsorbed phase is still in solid state, whereas the part near to the pore mouth is definitely liquidlike. One can see that there is an adsorbed film of argon at the inner pore surface of the vaporlike region without any ordering along the pore wall.

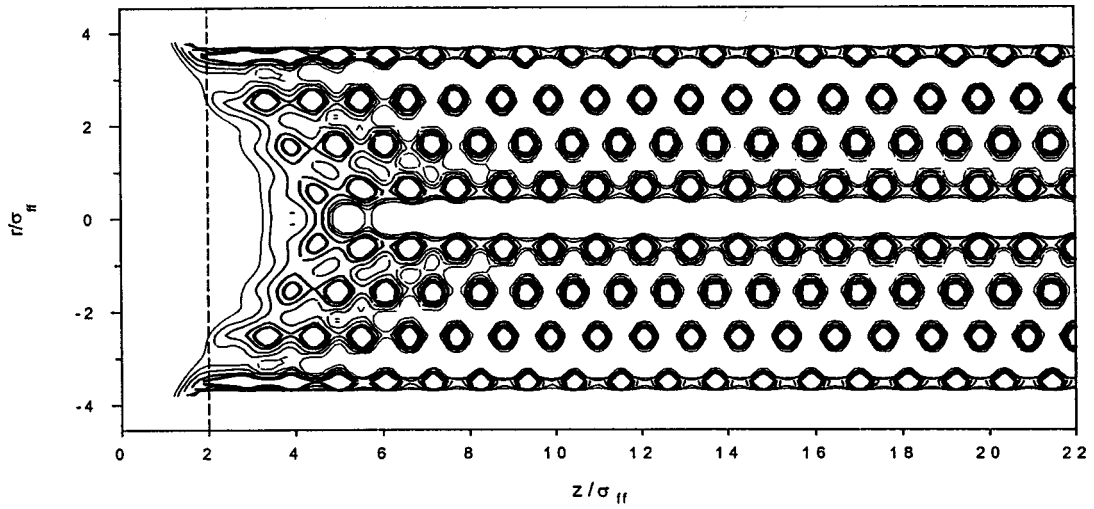

FIG. 5. Density distribution of solidified argon adsorbed in cylindrical pore of 3 nm at 87.3 K. Contour lines correspond to the following values of the specified local dimensionless density $\rho\sigma_{ff}^3$: 0.05, 0.1, 0.2, 0.5, 1. Average density of argon is 27 mmol/cm^3.

2. Isotherms in cylindrical pores and hysteresis in the case of freezing of argon

The molecular rearrangement with the formation of highly ordered structure that was considered in the preceding section has a significant consequence, which is reflected in the isotherm. Here we shall consider it in more detail. Figures 7(a) and 7(b) present argon isotherms for finite cylindrical pores of 3 and 4 nm diameters. Both have the same length (40 collision diameters). Dashed lines are calculated by canonical ensemble 1D NLDFT. Vertical dashed lines correspond to equilibrium vapor–liquid transition pressure, at which the grand potentials corresponding to the lower and upper points located on the adsorption and desorption liquid branches are equal. Circles denote liquidlike adsorption isotherms, which we obtained by suppressing the adsorbed phase to prevent crystallization as described in the preceding section. Squares (open for adsorption and filled for desorption) correspond to the case where we allowed crystallization in the adsorbed phase. What is interesting is that in the latter case evaporation occurs at lower pressure compared to that calculated for the uniform liquidlike structure of the adsorbed phase. One can see that at loadings up to the vaporlike spinodal point solutions corresponding to suppressing the adsorbed phase are the same as those when we do not suppress it. It means that crystallization does not occur in this low loading region and the adsorbed phase has the form of liquidlike films spreading over the inner pore surface. After the spinodal point has been reached, the pressure sharply decreases to vapor–liquid equilibrium pressure, indicating the coexistence of vapor and liquid. Further small increase of amount adsorbed does not immediately lead to crystallization and the equilibrium pressure holds at approximately the vapor–liquid transition pressure. Then the molecular rearrangement suddenly occurs and instead of further liquid filling the central part of the pore the solid phase appears. At this moment the pressure shifts to the lower level, corresponding to the vapor–solid coexistence. Further increase of loading nearly does not affect the equilibrium pressure until

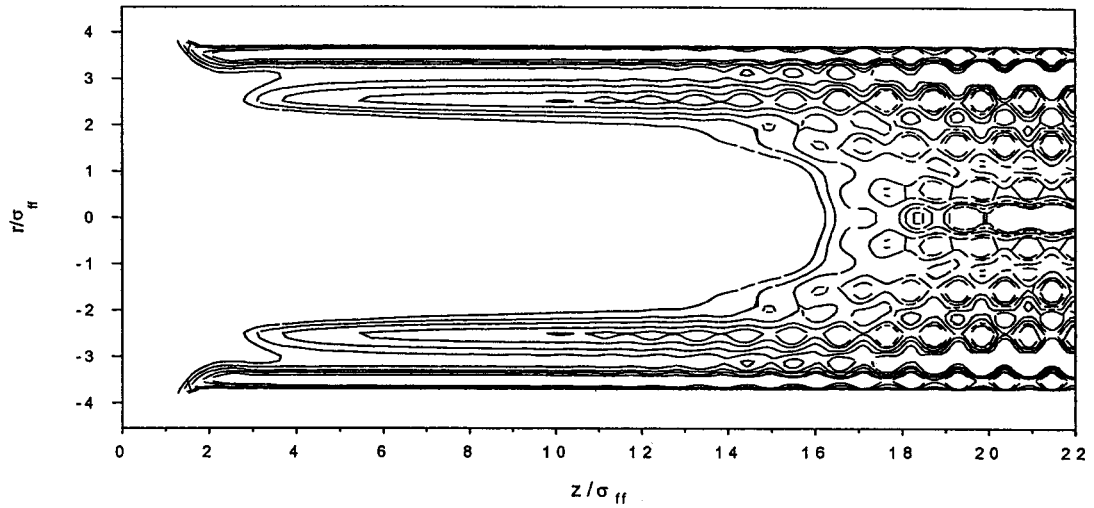

FIG. 6. Structure of argon adsorbed in cylindrical pore of 3 nm at 87.3 K. The average density of argon is 17 mmol/cm^3. Other conditions are the same as in Fig. 5.

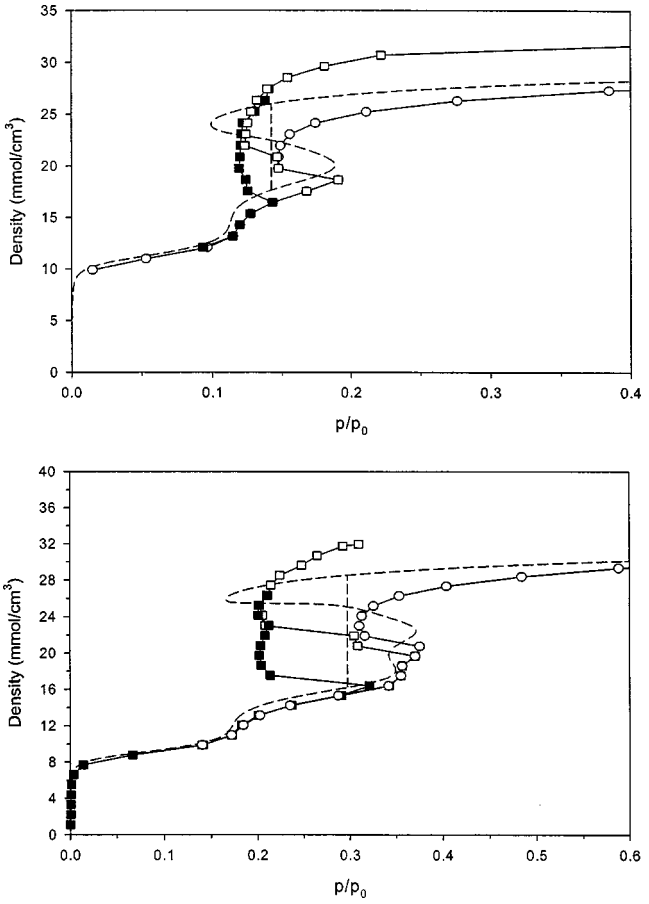

FIG. 7. Argon isotherms in finite cylindrical pore of (a) 3 nm and (b) 4 nm diameter at 87.3 K. The length of pores is 40 σ_{ff} (13.22 nm). Dashed lines, calculation by 1D NLDFT for the infinite pore. Circles, case when adsorbate is artificially kept in liquidlike state. Squares, case when adsorbed fluid can be spontaneously crystallized.

the pore is completely packed with molecules. Any further increase in the amount adsorbed leads to an increase of pressure. This part of the isotherm is higher than that corresponding to the ''artificially'' liquid adsorbed phase because of the higher density of the solid argon. The upper and lower parts of the desorption branch (filled square symbols) nearly coincide with those for the adsorption branch of the isotherm. However, we see that the vertical part of desorption branch is extended to significantly lower loading. It means that the solidlike adsorbed fluid filling the central part of the pore shrinks with the decrease of the total amount of argon in the pore but still maintains its integrity. At a critical value of the amount adsorbed the solidlike central part of the adsorbed phase becomes unstable and completely sublimes. The pressure abruptly increases and exactly falls on the adsorption branch. This corresponds to the situation where the adsorbed phase has become liquidlike and uniformly (with the exception regions close to open ends of the pore) distributed over the pore walls in the form of thin film.

Such a behavior of the adsorbed argon observed so far allows us to suggest the following mechanism for adsorption of argon in a cylindrical pore. In the early stage of adsorption, argon adsorbs uniformly along the pore and the adsorbed phase is liquidlike film adjacent to the solid surface. When the pressure approaches the vaporlike spinodal point the adsorbed phase becomes unstable and it splits into two phases. The first phase is in the central part of the cylindrical pore and the cross section of this part is completely filled with argon molecules in liquidlike state. The other phase is near the pore entrance where the adsorbed film remains on the pore wall, and the core of this section is vaporlike and it contributes negligibly to the total amount adsorbed. This split could occur before the vaporlike spinodal point is reached due to fluctuations in the density of the liquidlike film. In sufficiently narrow pores the adsorbed phase could divide into two phases at equilibrium transition pressure because the potential barrier could be easily overcome due to the fluctuations. Once appeared, the dense phase is in the form of a bridge, which is liquidlike because the molecular ordering is a relatively slow process. Once it is formed the bridge will spontaneously expand because this growth is thermodynamically favorable. In the open (grand canonical) system this process occurs at constant pressure until the pore volume is completely filled with liquidlike fluid. Rapid exchange of mass with the surrounding creates a disturbance, which hinders the crystallization. However, this process will start after the pore is filled. The molecular rearrangement and transformation of the liquidlike phase into the solidlike phase will lead to an increase in the amount adsorbed. Further increase of the bulk phase pressure will increase slightly the adsorbed phase density due to small compressibility of the frozen argon and tighter molecular packing at the pore ends.

Desorption will occur by another mechanism after the bulk pressure falls to the vapor–liquid equilibrium transition point. At this point the adsorbed phase remains solidlike, which is thermodynamically more favorable. Hence, the evaporation does not occur at this point and the bulk pressure will drop to a lower value, which conforms to the solid–liquid coexistence. This point is the actual pressure of equilibrium transition at which evaporation takes place until the amount adsorbed reaches the adsorption branch of the isotherm. The hysteresis loop in this case is bounded by the pressure of equilibrium solid–fluid transition on the left-hand side and equilibrium vapor–liquid transition pressure on the right-hand side. Of course, in larger pores the capillary condensation pressure will shift toward the vaporlike spinodal point due to the increase of the potential barrier, which could not be overcome readily by density fluctuations. On the other hand, in smaller pores the hysteresis loop described above could disappear due to more intensive and rapid crystallization, which gives rise to spontaneous filling of the pore volume with solidlike fluid without the intermediate formation of liquidlike phase. This hypothetical mechanism probably could be realized in pores with smoothed wall surface like graphite. The most attractive adsorbents to analyze described features by means of NLDFT are activated carbon and carbon nanotubes. In the case of siliceous adsorbents like MCM-41 the amorphous pore wall surface probably prevents molecular ordering of the adsorbed phase.

B. Argon adsorption in infinite cylindrical pores

Adsorption in infinite cylindrical pores may be considered as a limiting case of adsorption in finite pores. However,

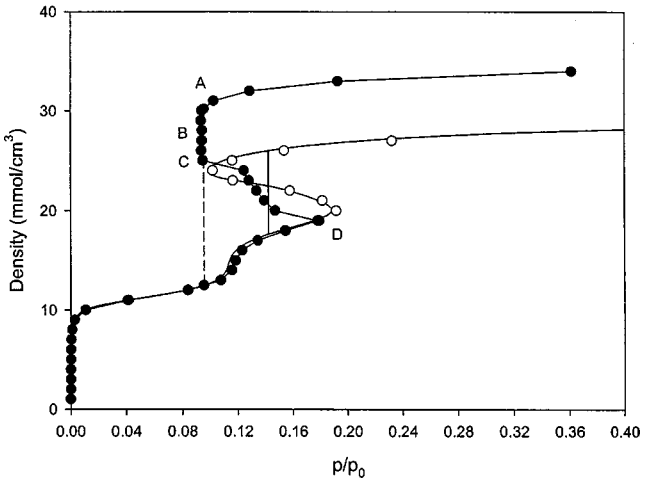

FIG. 8. Argon isotherm in infinite cylindrical pore of 3 nm diameter at 87.3 K. Opened circles, adsorption; filled circles, desorption. Vertical lines designate vapor–liquid (solid line) and solid–liquid (dashed line) phase transition, respectively.

the former case is an idealization of a real pore and it is not known *a priori* whether the absence of the pore edges and meniscus from the consideration does lead to any significant change in the adsorbed phase behavior or not. In this section we consider solution of the 2D NLDFT using a cylindrical cell with *mirror image* boundary conditions to simulate an infinite pore. The solid–fluid potential defined by Eq. (4) is valid for infinitely long cylinder. In the case of solidlike adsorbed phase the cell must have an integer number of periods of the density oscillation. Consequently, the distance between neighboring molecules depends on the cell length. This dependence decreases with an increase of the cell length, but at the expense of high computation cost. We compromise this by taking a cell length of about 10 collision diameters and then adjusting this length to minimize the Helmholtz free energy. As a general rule, it was sufficient to perform this adjustment once for a completely filled pore at a given pore diameter. Initial conditions are chosen to study the onset of adsorption and desorption branches. In the case of adsorption branch the initial distribution was uniform with a relatively small amount adsorbed (about 1 mmol/cm^3). Once the equilibrium is achieved, the amount adsorbed increases, with the equilibrium density distribution of the previous loading was taken as the initial condition for the calculation of the next loading. In the case of desorption branch we initiated crystallization by using an initial sinusoidal density distribution along radial and axial directions. This procedure does not produce any artifacts, because the initial density oscillations would disappear if the equilibrium uniform distribution (along the axis) is thermodynamically favorable.

Results of application of the 2D NLDFT to argon adsorption in infinite pore of 3 nm diameter are shown in Fig. 8. Adsorption branch of the isotherm calculated by 2D NLDFT (open circles) completely coincides with the solution obtained for one-dimensional case (solid line) over the full range of pressure. Hence, during adsorption the adsorbed phase is liquidlike despite the solid configuration is thermodynamically favorable. That is because density functional theory does not reproduce any effects associated with fluctuations. By this reason the adsorbed phase resembles a supercooled liquid. Formation of the solidlike adsorbed phase requires some initiation. In the case of finite pore the process of crystallization is induced by the presence of the meniscus, which is absent in the case of infinite pore. The desorption branch (filled circles) was started from the crystalline form of the adsorbed argon occupying the whole pore volume. It is seen from the figure that the density of the solidlike argon is higher compared to the liquidlike argon. Decrease of the amount adsorbed leads to the sharp decrease of the reduced pressure until it approaches a characteristic value of about 0.094, which is less than the equilibrium vapor–liquid transition reduced pressure (0.1424). This characteristic pressure of 0.094 remains constant when the argon loading is reduced from 30 to 25 mmol/cm^3 (point *A* to *C*). This is an indication of phase coexistence. Further decrease of loading leads to an increase in pressure towards vapor–liquid transition pressure. When the loading is less than approximately 20 mmol/cm^3, the pressure suddenly increases and falls on the adsorption metastable branch of the isotherm. At lower amount adsorbed the isotherm is reversible.

The sequence of Figs. 9(a)–9(f) shows the evolution of the adsorbed phase state with the decrease of argon amount adsorbed. At high average density of 31 mmol/cm^3 (point *A* on Fig. 8) the adsorbed phase is highly ordered as shown in Fig. 9(a). Molecules are packed in hexagonal solidlike structure. Figure 9(b) is plotted for a lower average density (28 mmol/cm^3), which corresponds to point *B* on the middle of the vertical part of the desorption branch in Fig. 8. This figure shows that the structure in the core of the pore has changed and become smoother, indicating formation of liquidlike structure in the proximity of the pore axis. This is further manifested in Fig. 9(c) for the argon density of 25 mmol/cm^3 (point *C* on the isotherm of Fig. 8). The fluid in the core of the pore is completely melted, whereas it is still solidlike close to the pore walls. Hence one can conclude that the vertical part of the desorption branch of the isotherm corresponds to the solid–liquid phase transition. The density oscillates along the axis with the period of about one collision diameter, but there are no long-range oscillations with the formation of a meniscus. It means that the adsorbed phase has split into solid and liquid regions along the radial direction, and the interface is parallel to the pore walls. The pressure of the solid–liquid coexistence is nearly the same in relatively wide range of the amount adsorbed. Interestingly when the average density becomes lower than a critical value, the liquidlike phase is evolved along the axial direction into the vaporlike and the solidlike phase [Fig. 9(d)]. Before the liquidlike phase was broken it was in a highly stretched state, which did not allow it to be organized in an ordered solidlike structure. The appearance of meniscus sharply decreases the longitudinal stress, and the part of fluid that was in liquidlike state (as a result of melting during the decrease of loading) again solidifies. The state of argon adsorbed at the pore wall in the part of pore with empty core is somewhat ordered, but it could be resulted from not sufficient length of the cell (only 10 collision diameters). Never-

theless, the appearance of two phases along axial direction does not correspond to the vapor–liquid coexistence. Rather, this is the case of vapor–solid coexistence, which conforms to a lower pressure compared to that for the vapor–liquid coexistence. The decrease of amount adsorbed leads to the expansion of the vaporlike phase and the shrinkage of the solidlike phase within the core, which is accompanied by apparent melting of this part [Fig. 9(e)]. Thus, the vapor–solid coexistence is gradually shifted to the vapor–liquid coexistence. At a critical value of the average density the core is completely vaporized and the density distribution along the pore axis becomes uniform [Fig. 9(f)]. This point corre-

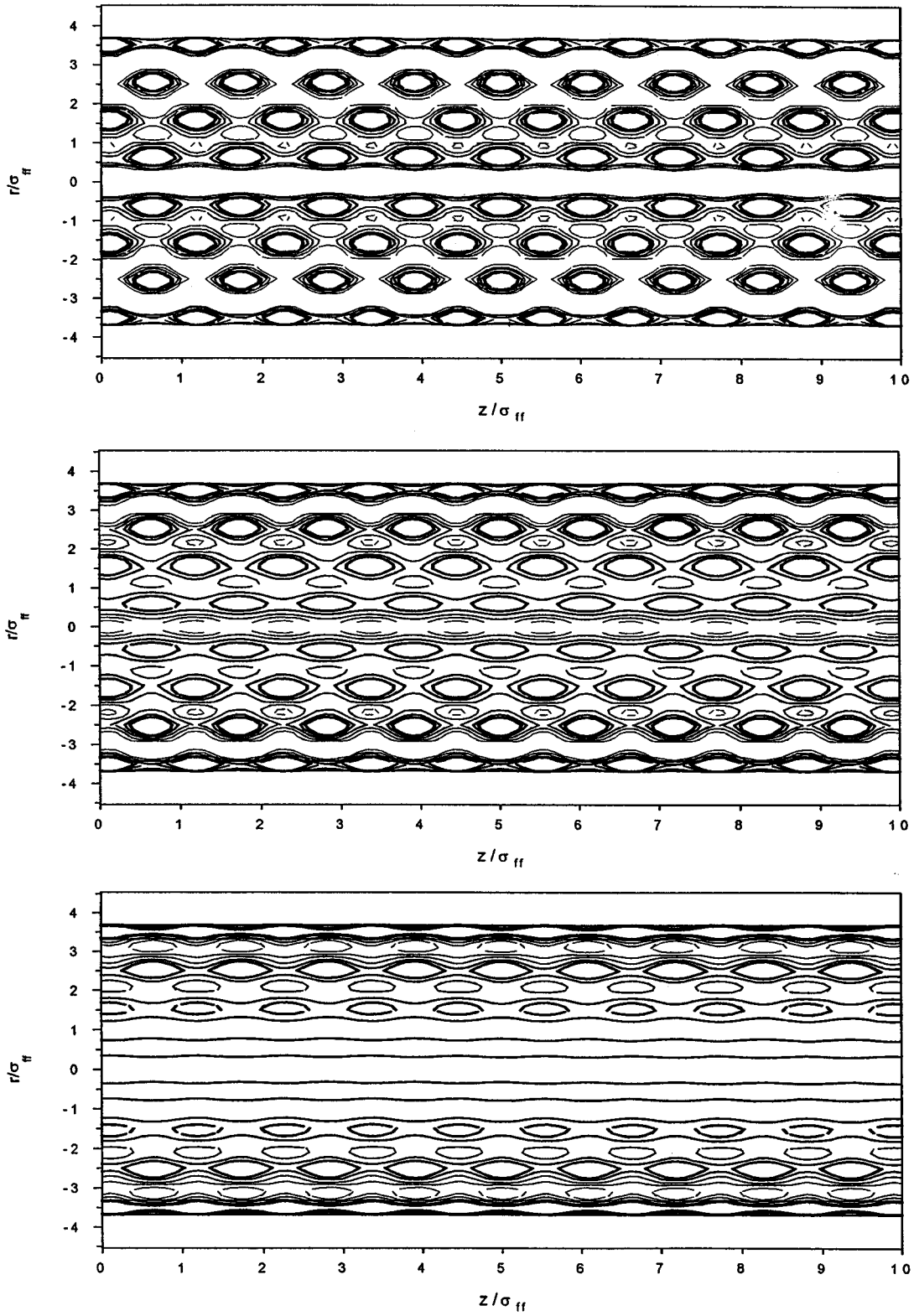

FIG. 9. Density profile of argon in infinite pore of 3 nm diameter at 87.3 K. Amount adsorbed, mmol/cm^3: (a) 31, (b) 28, (c) 25, (d) 24, (e) 21, (f) 19. Figure shows the development of desorption.

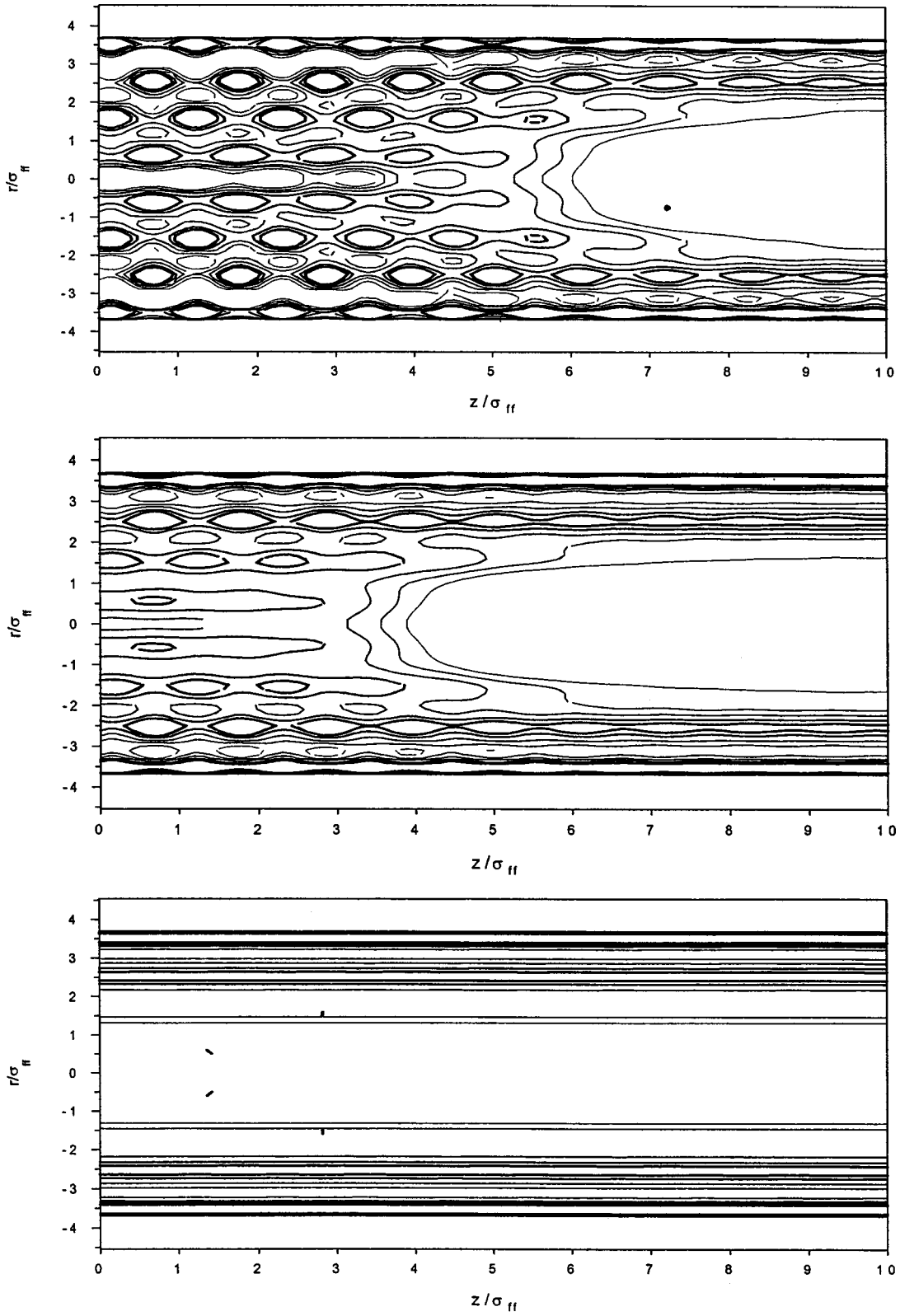

FIG. 9. (*Continued.*)

sponds to the metastable branch of the adsorption isotherm (point *D* of Fig. 8).

Further investigations are needed to determine effect of the pore diameter and temperature on the state of adsorbed phase and phase transition. It is also necessary to check the applicability of the Tarazona's version of density functional theory and the mean field approximation to the case of highly ordered structure of fluids both in the bulk phase and in confined space of the pore volume of adsorbents. Another aspect worthwhile of further study is the application of the density functional theory to deal with surface roughness, as in case of siliceous adsorbents.

V. CONCLUSION

We present the application of the two-dimensional version of the nonlocal density functional theory (2D NLDFT) to analyze adsorption and desorption of argon in cylindrical pores at 87.3 K. Finite pores as well as infinite pores were considered in this paper. The new features resulting from this analysis (which are not observed in the simpler 1D NLDFT, commonly applied in the literature) are the formation of solid phase and the complex transition between the various possible phases in the system, vapor, liquid, and solid phases. The formation of solid in the pore may be a possible reason for hysteresis commonly observed experimentally. Further analysis is needed to check the applicability of density functional theory based on the mean field approximation to nonuniform axial distribution of fluids adsorbed in cylindrical pores and to description of their solidification.

ACKNOWLEDGMENT

Support from the Australian Research Council is gratefully acknowledged.

APPENDIX: SOLID-FLUID POTENTIAL ENERGY FOR A FINITE CYLINDER

Let us consider a finite cylindrical layer of radius R and length L. In order to calculate potential at the point with coordinates r and z along the radial and longitudinal directions, respectively, we need first to write the pair potential exerted by an atom residing at the surface and having the coordinate $z'=z+z_1$. If we define α as the projection angle between the radius vectors $\mathbf{r}$ and $\mathbf{r}'$ on the plane of constant z, the distance between the two given points is

$$x=(R^2+r^2+z_1^2-2rR\cos\alpha)^{1/2}. \tag{A1}$$

If we assume that the pair potential can be described by a classical Lennard-Jones 12-6 potential, the potential energy between the two given points is

$$u'=4\epsilon_{sf}\left[\frac{\sigma_{sf}^{12}}{x^{12}}-\frac{\sigma_{sf}^{6}}{x^{6}}\right]. \tag{A2}$$

The potential energy between the given atom and the surface is then obtained by appropriately integrating Eq. (A2) with respect to z_1 ($-z\leqslant z_1\leqslant L-z$) and α ($0\leqslant\alpha\leqslant 2\pi$). The integral with respect to z_1 can be readily obtained analytically. First, we consider the following integral:

$$\int_0^z \frac{dz_1}{R^2+r^2+z_1^2-2rR\cos\alpha}=\frac{1}{\sqrt{g}}\operatorname{arctg}\left(\frac{z}{\sqrt{g}}\right), \tag{A3}$$

where

$$g=R^2+r^2-2rR\cos\alpha. \tag{A4}$$

Repeated differentiation of Eq. (A3) with respect to g yields the following expression:

$$f_n(z,r,R,\alpha)=\int_0^z \frac{\sigma_{sf}^{2n-1}\,dz_1}{(g+z_1^2)^n}=\frac{(-1)^{n-1}\sigma_{sf}^{2n-1}}{(n-1)!}\frac{d^{n-1}}{dg^{n-1}}\left[\frac{1}{\sqrt{g}}\operatorname{arctg}\left(\frac{z}{\sqrt{g}}\right)\right]. \tag{A5}$$

In the general case the function $f_n(z)$ can be represented as follows:

$$f_n(z,r,R,\alpha)=\frac{\sigma_{sf}^{2n-1}}{2^{n-1}(n-1)!g^n}\times\left\{(2n-3)!!\,g^{1/2}\operatorname{arctg}(zg^{-1/2})+z\sum_{k=1}^{n-1}b_{n,k}g^k(z^2+g)^{-k}\right\}, \tag{A6}$$

where coefficients $b_{n,k}$ for $n\geqslant 3$ are obtained from the following recurrent equations:

$$b_{n+1,k}=2(n-k)b_{n,k}+2(k-1)b_{n,k-1},\quad k\geqslant 2,$$
$$b_{n+1,1}=2(n-1)b_{n,1}+(2n-3)!! \tag{A7}$$

Here $b_{2,1}=1$.

Having obtained the necessary equation (A5), we can integrate the potential energy with respect to z_1 and α. The part of integration with respect to z_1 is

$$\int_0^z u'(z_1,r,R,\alpha)dz_1=4\epsilon_{sf}\sigma_{sf}[f_6(z,r,R,\alpha)-f_3(z,r,R,\alpha)]. \tag{A8}$$

The second integral with respect to α can be readily obtained numerically. Finally, we can obtain the following expression in the case of finite cylinder having length L:

$$u(z,r,L,R)=\rho^s R\int_0^L\int_0^{2\pi}u'(z_1,r,R,\alpha)d\alpha\,dz_1=8\rho^s\epsilon_{sf}\sigma_{sf}R\times\int_0^{\pi}[f_6(z,r,R,\alpha)+f_6(L-z,r,R,\alpha)-f_3(z,r,R,\alpha)-f_3(L-z,r,L,\alpha)]d\alpha. \tag{A9}$$

In the case of infinite cylindrical pore the contribution of the sum on the right-hand side of Eq. (A6) is zero and $\operatorname{arctg}(zg^{-1/2})$ is $\pi/2$ and we obtain

$$u(r,R)=3\pi\rho^s\epsilon_{sf}\sigma_{sf}R\int_0^{\pi}\left[\frac{21}{32}\frac{\sigma_{sf}^{11}}{g^{11/2}}-\frac{\sigma_{sf}^{5}}{g^{5/2}}\right]d\alpha. \tag{A10}$$

[1] J. S. Beck, J. C. Vartuli, W. J. Roth *et al.*, J. Am. Chem. Soc. **114**, 10834 (1992).
[2] D. Khushalani, A. Kuperman, G. A. Ozin, K. Tanaka, J. Garces, M. M. Olken, and N. Coombs, Adv. Mater. (Weinheim, Ger.) **7**, 842 (1995).
[3] Q. Huo, D. I. Margolese, and G. D. Stucky, Chem. Mater. **8**, 1147 (1996).
[4] P. Tarazona, Phys. Rev. A **31**, 2672 (1985).
[5] R. Evans, U. M. B. Marconi, and P. Tarazona, J. Chem. Soc., Faraday Trans. 2 **82**, 1763 (1986).

[6] P. Tarazona, U. M. B. Marconi, and R. Evans, Mol. Phys. **60**, 573 (1987).
[7] N. A. Seaton, J. P. R. B. Walton, and N. Quirke, Carbon **27**, 853 (1989).
[8] C. Lastoskie, K. E. Gubbins, and N. Quirke, J. Phys. Chem. **97**, 4786 (1993).
[9] C. Lastoskie, K. E. Gubbins, and N. Quirke, Langmuir **9**, 2693 (1993).
[10] J. P. Olivier, J. Porous Mater. **2**, 9 (1995).
[11] J. P. Olivier, Carbon **36**, 1469 (1998).
[12] A. V. Neimark and P. I. Ravikovitch, Langmuir **13**, 5148 (1997).
[13] P. I. Ravikovitch, A. Vishnyakov, R. Russo, and A. V. Neimark, Langmuir **16**, 2311 (2000).
[14] J. C. P. Broekhoff and J. H. de Boer, J. Catal. **9**, 8 (1967); **9**, 15 (1967).
[15] J. C. P. Broekhoff and J. H. de Boer, J. Catal. **10**, 368 (1968); **10**, 377 (1968); **10**, 391 (1968).
[16] A. V. Neimark, P. I. Ravikovitch, and A. Vishnyakov, J. Phys.: Condens. Matter **15**, 347 (2003).
[17] L. H. Cohan, J. Am. Chem. Soc. **60**, 433 (1938).
[18] E. P. Barrett, E. G. Joyner, and P. H. Halenda, J. Am. Chem. Soc. **73**, 373 (1951).
[19] A. V. Neimark and P. I. Ravikovitch, Microporous Mater. **44–45**, 697 (2001).
[20] M. Kruk, M. Jaroniec, and A. Sayari, Langmuir **13**, 6267 (1997).
[21] M. Kruk, V. Antochshuk, M. Jaroniec, and A. Sayari, J. Phys. Chem. B **103**, 10670 (1999).
[22] M. Kruk and M. Jaroniec, Chem. Mater. **12**, 222 (2000).
[23] M. W. Cole and W. F. Saam, Phys. Rev. Lett. **32**, 985 (1974).
[24] D. H. Everett, in *The Solid–Gas Interface*, edited by E. A. Flood (Decker, New York, 1967).
[25] M. Kruk, M. Jaroniec, and A. Sayari, Adsorption **6**, 47 (2000).
[26] S. J. Greg and K. S. W. Sing, *Adsorption, Surface Area and Porosity* (Academic, London, 1982).
[27] M. Kruk and M. Jaroniec, Chem. Mater. **13**, 3169 (2001).
[28] P. I. Ravikovitch, A. Vishnyakov, and A. V. Neimark, Phys. Rev. E **64**, 011602 (2001).
[29] A. Vishnyakov and A. V. Neimark, J. Phys. Chem. B **105**, 7009 (2001).
[30] A. Vishnyakov and A. V. Neimark, J. Chem. Phys. **118**, 7585 (2003).
[31] L. D. Gelb, Mol. Phys. **100**, 2049 (2002).
[32] A. V. Neimark and P. I. Ravikovitch, "Density functional theory for studies of multiple states of inhomogeneous fluids at solid surfaces and in pores," in *Microscopic Simulation of Interfacial Phenomena in Solids and Liquids*, edited by S. L. Phillpot, P. D. Bristowe, D. G. Stroud, and J. R. Smith (Materials Research Society, Warrendale, PA, 1998), Vol. 492, pp. 27–33.
[33] P. I. Ravikovitch and A. V. Neimark, Colloids Surf., A **187–188**, 11 (2001).
[34] P. I. Ravikovitch and A. V. Neimark, J. Phys. Chem. B **105**, 6817 (2001).
[35] J. D. Weeks, D. Chandler, and H. C. Andersen, J. Chem. Phys. **54**, 5237 (1971).
[36] N. F. Carnahan and K. E. Starling, J. Chem. Phys. **51**, 635 (1969).
[37] R. Evans, in *Fundamentals of Inhomogeneous Fluids*, edited by D. Henderson (Marcel Dekker, New York, 1992), Chap. 5.
[38] G. J. Tjatjopoulos, D. L. Feke, and J. A. Mann, J. Phys. Chem. **92**, 4006 (1988).
[39] A. V. Neimark, P. I. Ravikovitch, M. Grün, F. Schüth, and K. K. Unger, J. Colloid Interface Sci. **207**, 159 (1998).
[40] K. Kaneko, A. Watanabe, T. Iiyama, R. Radhakrishnan, and K. E. Gubbins, J. Phys. Chem. B **103**, 7061 (1999).
[41] L. D. Gelb, K. E. Gubbins, R. Radhakrishnan, and M. Sliwinska-Bartkowiak, Rep. Prog. Phys. **62**, 1573 (1999).
[42] M. W. Maddox and K. E. Gubbins, J. Chem. Phys. **107**, 9659 (1997).
[43] S. Granick, Science **253**, 1374 (1991).
[44] H. W. Hu, G. A. Carson, and S. Granick, Phys. Rev. Lett. **66**, 2758 (1991).
[45] J. Klein and E. Kumacheva, Science **269**, 816 (1995).